Characterization of the volume fraction of soft deformable microgels by means of small-angle neutron scattering with contrast variation

Andrea Scotti [a*]

The volume occupied by colloids in a suspension - namely the volume fraction - is the thermodynamic variable that determines the phase behavior of these systems. While for hard incompressible spheres this quantity is well defined, for soft compressible colloids such as microgels - polymeric crosslinked networks swollen in a good solvent - the determination of the real volume occupied by these particles in solution is particularly challenging. This fact depends on two aspects: first the surface and, therefore, the volume of the microgels is hard to define properly given their external fuzziness; second, microgels can osmotically deswell, deform or interpenetrate their neighbors, i.e. change their shape and size depending on the solution concentration. Here, the form factors of few hydrogenated microgels embedded in a matrix of deuterated but otherwise identical microgels are measured using small-angle neutron scattering with contrast variation. From the analysis of the scattering data, the variation of the volume of the microgels as a function of concentration is obtained and used to calculate the real microgel volume fraction in solution. Soft neutral microgels are shown to facet already at low concentrations while in contrast, harder microgels maintain their shape and change their volume.

1 Introduction

Colloidal suspensions of soft compressible microgels, crosslinked polymeric networks swollen in a good solvent, have been widely used to study both phase transitions [1–3], glass formers [4–7] and the rheological properties of complex fluids [8–10]. In contrast to hard spheres, microgels allow the role of softness on the properties of complex materials to be investigated. Furthermore, the polymer composing the network of the microgels goes through a coil-to-globule transition depending on the variation of external stimuli, such as temperature or pH [11–13]. As a consequence of this transition, the microgel volume can be finely tuned on demand. This is particularly appealing since it offers the possibility to change the volume occupied by the microgels in a single solution just, for instance, by varying the temperature [1,8].

The common way to think of colloidal suspensions is to use the same formalism used in the description of atomic systems. For instance, the equation of state for a dilute colloidal suspension can be written as $\pi v_0 = k_B T \phi$ where π is the osmotic pressure of the colloidal suspension, k_B is the Boltzmann constant, T is the temperature, and v_0 and ϕ are the volume of a single colloid and the volume occupied by the colloids in the suspension, respectively. The latter can be rewritten as

$$\phi = \frac{v_0 N}{V} \tag{1}$$

where N and V are the total number of colloids in suspension and the total volume of the suspension, respectively. However, when the concentration of colloids increases things become more complicated and the ideal gas law cannot describe the system anymore. Though, the important variables for the equation of state of the suspension, known as Carnahan-Starling equation [14], are π, ϕ and T. In general, at constant temperature, the phase behavior and flow properties of the solution are completely determined by the value of ϕ [1,3,6,10,15].

For these reasons it is fundamental to know precisely the value of the volume occupied by the colloids in solution, the volume fraction ϕ. When the colloids are spheres with a well defined volume, v_0, this can be determined by means of dynamic light scattering. Then, the density of the material of which these particles are composed can be used to compute the mass of a single particle $m = v_0/\rho$. This value can be used to divide the total mass of particles added in suspension to obtain their number N and, therefore, their volume fraction ϕ. We note that already in the pioneering work of Pusey and van Megen [15], the authors warn about the difficulties of having truly hard and incompressible spheres. More recently, a critical review that compared experiments on hard colloids to theory and computer simulations highlighted that there are systematic errors in the values of ϕ determined experimen-

[a] *Institute of Physical Chemistry, RWTH Aachen University, 52056 Aachen, Germany*
[*] *Email: andrea.scotti@rwth-aachen.de*

tally which cannot be eliminated[16], and have always to be considered.

The situation becomes more complicated as colloidal particles become increasingly soft. For instance, it is very challenging to compute the real value of the volume fraction ϕ of solutions of microgels. Indeed, in addition to the intrinsic errors highlighted in the literature[16], there are two other main reasons that make hard the determination of ϕ: (i) microgels possess a fuzzy external shell composed of dangling polymeric chains which makes hard to clearly define their volume[11]; (ii) microgels changes their volume and/or shape once the concentration increases[17–19]. This is due to the fact that a larger number of microgels in solution implies a larger number of counter-ions associated to these particles which can leave the microgel and increase the suspension osmotic pressure[7,20,21]. As soon as π is comparable to the microgel bulk modulus an osmotic deswelling is observed[22]. In addition to this mechanism, microgels can also facet and deform[18] or interpenetrate their neighbors[23]. Due to these considerations, it is clear that the problem is to determine the value of v_0 for microgels in Equation 1.

An alternative to the use of ϕ is to use the so-called generalized volume fraction, ζ, where the value of v_0 is fixed to the volume of the microgels in the limit of highly diluted samples[1,2,6,24]. The relation $\phi = \zeta$ holds as long as the volume of the microgels do not change, that is usually the case for low concentrations. The values of ζ can rise well above the limit of maximum packing for hard spheres in random and ordered arrangement, $\phi_{rcp} = 0.64$ and $\phi_{cp} = 0.74$, respectively. In general, ζ can assume values well above the unit which implies that the microgels in solution have significantly changed their volume or shape. Still, the problem of relating ζ to the real volume occupied by the microgels in solution, that is ϕ, is unsolved.

Recently, an elegant solution to address this problem has been presented for ionic microgels[21,25]. The key point is that, as mentioned above, the equation of state relates the suspension osmotic pressure, π, to the value of ϕ, and not ζ. The value of the osmotic pressure of the suspension is set up by the counter-ions that can leave the microgels for entropic reasons and can be directly measured both with osmotic stress solutions[21,25] or by means of a membrane osmometer[21,22]. Then using the relation between osmotic pressure, free counter-ions and ϕ developed by Cloitre and coworker[7,20] it is possible to map the values of $\pi(\zeta)$, measured experimentally, over the expected values of $\pi(\phi)$ and finally obtain the real volume fraction of the microgels in suspension[21,25].

A second way to tackle this problem is to directly measure the volume of the microgels as a function of the generalized volume fraction and use this to rescale ζ into ϕ. This can be done both in real space in principle by means of super resolved florescent microscopy (SRFM)[18,24,26–28], or in the reciprocal space by means of small-angle neutron scattering with contrast variation[3,19,23,29,30]. SRFM typically requires microgels immobilized during the time in which the images are acquired. This has been shown to be possible at relatively high concentrations[18,24,31] while for diluted or semi-diluted samples the microgels must be adsorbed and immobilized at the solid liquid interface. The adsorption of microgels at interfaces leads to their deformation[32] and in principle the elastic properties and the dimensions differ from the one of the microgels in bulk[32–34]. Furthermore, the addition of of salt, typically mercaptoethylamine[18,24,31] to induce the blinking of the dye limits the experimental conditions at which super-resolved fluorescent microscopy can be performed.

Small-angle neutron scattering (SANS) with contrast variation is the method used in this study to access the volume of microgels in concentrated solutions. In the past years, SANS with contrast variation has largely been used to explored the response of the internal structure of microgels to crowded environments. It has been found that when microgels with different bulk moduli are mixed together the external shell of the softest microgels deswell first. This is the case for mixture of larger and smaller microgels[22] for mixture of softer microgels embedded in matrix of harder one with comparable dimensions[19] and for mixture of microgels with comparable size but different internal structures, e.g. regular and hollow microgels[19,35]. Once microgels with comparable bulk moduli and dimensions are mixed together, it has been observed a competition between osmotic deswelling - which mainly collapse the external shell - and faceting/interpenetration - where the microgels decrease in size maintaining a certain fuzziness and interpenetrate the neighbors. This has been observed for solution of regular microgels[19,23,29,30], ultra-low crosslinked microgels[3], and hollow-microgels[36]. In contrast to these previous study, here the total radius of hydrogenated microgels embedded in a matrix of deuterated, but otherwise identical, microgels is used to map the microgel generalized volume fraction on ϕ. The experiments have been conducted on suspensions of 5 mol% crosslinked[19] and ultra-low crosslinked microgels[3,37] to probe the effect of different network topologies on the response of individual microgel. Depending on the amount of crosslinker agent used during the synthesis the onset for faceting and osmotic deswelling happens at different concentrations.

2 Experimental

2.1 Synthesis

All the microgels used in this study are obtained by standard precipitation polymerization. The main monomer used is *N*-isopropylacrylamide (NIPAM) ($[C_6H_{11}NO]_n$) or deuterated monomers of NIPAM in which three or seven atoms of hydrogen have been substituted by deuterium.

The 5-mol% crosslinked microgels, the two hydrogenated and the deuterated one, have been synthesized according to standard precipitation polymerization with 5 mol% of crosslinker agent *N,N'*-methylenebisacrylamide (BIS). Surfactants have also been added during the synthesis to both control the final microgel size and the size polydispersity[38]. The detailed description of the synthesis procedure for these microgels can be found in the literature[19,33,37]. From now on we will refer to these microgels as regular microgels. The two different hydrogenated 5 mol% crosslinked microgels used here have been obtained from two different synthesis. They will be named $H,5\%-A$ and $H,5\%-B$, respectively, see Table 1. While for both the microgels the amount of crosslinker is fixed to 5 mol%, a small amount (2 mol%) of the co-monomer N-(3-aminopropyl)methacrylamide hydrochlo-

ride (APMH) has been added during the synthesis of $H,5\%-A$[33,39]. The incorporation of APMH allows to use these microgels for further study using covalent labeling with fluorescent dyes[31,40]. In contrast, the microgel indicated here as $H,5\%-B$ have been synthesized using only NIPAM monomers[19]. As a consequence of the different synthesis, $H,5\%-A$ and $H,5\%-B$ have slightly different swollen/collapsed sizes and stiffness.

The ultra-low crosslinked - ULC - microgels, both hydrogenated and deuterated, have been synthesized following a classic precipitation polymerization protocol but without the addition of crosslinker agents. Surfactants have also been added during the synthesis to both control the final microgel size and the size polydispersity[38]. The crosslinking of the polymeric networks is due to atom abstraction reactions during the polymerization of NIPAM initiated with a peroxydisulfate initiator[41]. More information on the synthesis of these ultra-low crosslinked microgels can be found in the literature[3,37,41].

Threefold centrifugation and redispersion in fresh water was applied for the purification of all the synthesized microgels. Samples were lyophilized for storage. It is well accepted since the first works of Pelton[42–44] that above the volume phase transition temperature microgels retain a significant quantity of water (approximately between 10 and 40% of the volume fraction). The conditions at which the lyophilization is performed, under vacuum, are the best that can be achieved to evaporate as much water as possible but still, it cannot be excluded that some residual water - likely $\lesssim 10\%$ - is still trapped within the "dry" microgels. The freeze-dried powder of the microgels was redispersed in pure double distilled milli-Q water, or in mixtures of pure double distilled milli-Q water and heavy water.

2.2 Viscosimetry

The viscosity of suspensions of hard spheres increases with increasing sphere packing fraction[45]. For small concentrations of spheres in suspension, in the limit of highly diluted samples, the Einstein-Batchelor equation well describes the course of η_r, the solution viscosity divided by the solvent viscosity, as a function of the sphere packing fraction, ϕ:

$$\eta_r = 1 + 2.5\phi + 5.9\phi^2 \tag{2}$$

In the literature it is shown that Equation 2 holds also for solutions of microgels in the limit of highly diluted samples[1,20]. The formal substitution of $\phi = \zeta$, true at low concentrations where the microgels do not experience any deswelling or deformation, allows us to write Eq. 2 for solutions of soft spheres: $\eta_r = 1 + 2.5\zeta + 5.9\zeta^2$. The generalized volume fraction is related to the microgel concentration in solution, c, by means of a multiplicative constant, k[1,2,7,18,22–24,29,46]. The value kc can be substituted in the previous equation to obtain $\eta_r = 1 + 2.5kc + 5.9(kc)^2$. This equation is used to fit the course of the relative viscosity of highly diluted solutions of microgels as a function of c. From the fits, the value of the conversion constant k and, therefore, the generalized volume fraction, is obtained. This method has been successfully used in the literature to compute the generalized volume fraction of microgels suspensions and describe both their equilibrium phase behavior[1,2,23,47] and their rheological properties[7,8,24].

The values of the solution kinematic viscosity are obtained by measuring the time of fall, t_{fall}, of a fixed volume of the solution through a thin glass capillary in an Ubbelohde tube viscometer immersed in a water bath at a fixed temperature of $(20.0\pm0.1)\,^{\circ}$C. The time of fall is connected to the solution kinematic viscosity by means of a conversion constant that depends on the geometrical characteristics of the capillary, C:, $\nu = Ct_{fall} = \eta/\rho_s$ where ρ_s is the density of the solution. Here ρ_s is assumed to be equal to the density of the pure solvent. This is justified by the low concentrations of polymer is solution, $c \ll 0.4$ wt%. Once $\eta = Ct_{fall}\rho_s$ is computed it is divided for the solvent viscosity, η_s, to obtain the relative viscosity.

2.3 Small-angle neutron scattering

2.3.1 Contrast variation

In a small-angle neutron scattering experiment the scattering vector is defined as $q = \frac{2\pi}{\lambda}\sin(\frac{\vartheta}{2})$ where λ is the wavelengths of the radiation (e.g. x-rays or neutrons) in the medium and ϑ is the scattering angle. The intensity measured, $I(q)$, is proportional to the squared value of the difference in scattering length density (or contrast) between the sample and the background, $\Delta\rho^2$, the particle form factor, $P(q)$, and the sample structure factor, $S(q)$. The form factor contains all the information on the single scattering object: shape of the object, internal structure, characteristic lengths. The structure factor is related to the particle-to-particle distance and gives information on the global arrangement of the samples. For instance $S(q)$ describes if a sample is in a fluid, disordered or crystalline phase, and can be used to distinguish the particular crystalline lattices formed[3,46,48]. In the limit of highly diluted samples, the structure factor can be approximated to one, and the scattered intensity is directly proportional to the square of the difference in scattering length density between the the solvent and the the microgels, $\Delta\rho^2$, multiplied by the form factor.

Depending on the radiation chosen, the contrast, $\Delta\rho$, depends on the interaction potential between the radiation itself and the sample. For instance, x-rays interact with the electron clouds of the atoms composing the samples *via* Coulomb interaction. In contrast, neutrons interact by means of the strong nuclear interaction with the nuclei of the atoms composing the sample. This fact has important experimental consequences: while the contrast for x-rays increases monotonically with the atomic number, the variation of the contrast for neutron scattering is unsystematic throughout the periodic table[49]. The difference in scattering length - or contrast - between hydrogen and deuterium is of particular interest for the soft matter community since it allows us to properly tune the contrast of the samples by means of the substitution of hydrogen atoms with atoms of deuterium. In this way, the contrast of the samples can be changed without significantly affecting their chemical composition. Then, by tuning the contrast of the solvent, for instance mixing water and heavy water, different parts of the sample can be contrast matched and become virtually invisible during the scattering experiment.

Table 1 Name of the samples, main monomer used for the microgels synthesis, amount of crosslinker agent - BIS - added during the precipitation polymerization, symbol used in all the Figures, hydrodynamic radii of the used microgels determined using multi-angle dynamic light scattering [3,19,33], R_h, and values of the conversion constant, k, as determined by the fits of the data in Figure 2 with the Einstein-Batchelor equation.

Name	Monomer	BIS (mol%)	Symbol	R_h (nm)	k
ULC_D	$[C_6D_3H_8NO]_n$	0	▲	138.3 ± 0.6	22.8 ± 0.5
ULC_H	$[C_6H_{11}NO]_n$	0	●	135 ± 1	44.8 ± 0.9
$D, 5\%$	$[C_6D_7H_4NO]_n$	5	□	153 ± 1	23.5 ± 0.5
$H, 5\% - A$	$[C_6H_{11}NO]_n$	5	♦	153.2 ± 0.5	17.0 ± 0.6
$H, 5\% - B$	$[C_6H_{11}NO]_n$	5	■	165 ± 4	11.2 ± 0.3

Neutron scattering with contrast variation is an ubiquitous technique to the structural characterization of single objects in soft matter for instance for bio-compatible materials[50,51], soft colloids[52] and microemulsions[53]. Commonly, a part of the single scattering object, e.g. a colloid composed by a rigid core and surrounded by a polymeric network, can be selectively contrast matched by choosing the proper mixture of water and heavy water[54]. A second possible way to take advantage of contrast variation and neutron scattering is schematically shown in Figure 1.

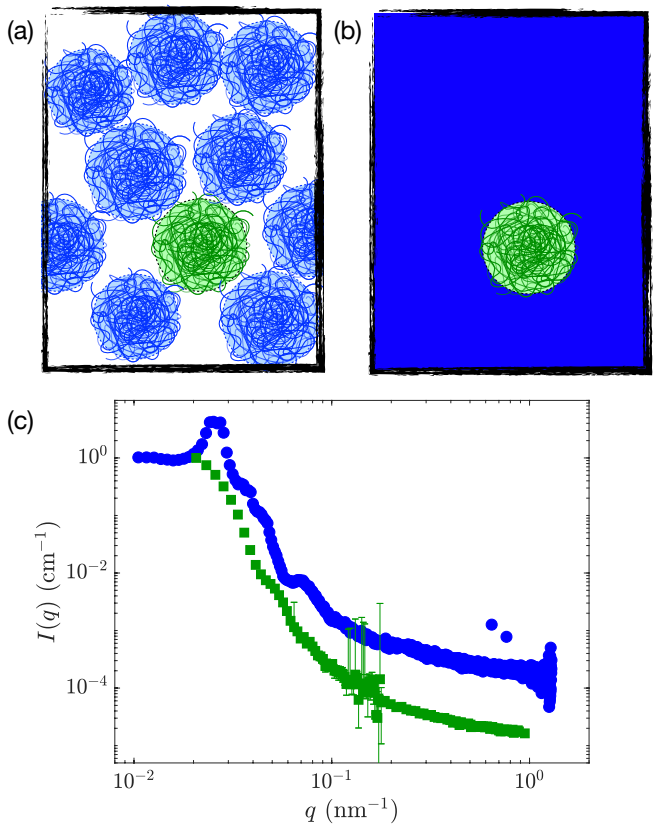

Fig. 1 (a) Sketch of a sample composed of a majority of deuterated (blue) and hydrogenated (green) particles (e.g. microgels). (b) Sketch of a sample composed of a majority of deuterated (blue) and hydrogenated (green) particles (e.g. microgels) in a solvent that is contrast matched to the scattering length density of the deuterated particles. (c) Small-angle x-ray (blue circles) and neutron scattering (green squares) intensities, $I(q)$, versus scattering vector, q.

The schematic in Figure 1(a) represents a sample composed by a mixture of deuterated (blue) and hydrogenated particles (green), such as microgels. When this sample is measured by small-angle x-ray scattering (SAXS) the contrast between all the particles and the background (white) is the same. As a consequence all the particles are visible and the measured scattered intensity is proportional to $S(q)P(q)$. Figure 1(b) shows a sketch of the very same sample measured with small-angle neutron scattering. If the solvent has been properly tuned, the contrast of the deuterated particles (blue) is matched by the solvent (blue) and these particles are "invisible" during the experiment. In such a sample only the form factor of the hydrogenated particles (green) is probed. An example of measured SAXS and SANS intensities (blue circles and green squares, respectively) is given in Figure 1(c). The $I(q)$ from SAXS presents oscillations and peaks but it is extremely complicate to distinguish which features of the curve are due to the single particle and which are due to the particle-to-particle arrangement. In contrast, the signal of the very same sample measured using SANS with contrast variation is proportional to the form factor of the hydrogenated particles and the measured curve depends only on the shape and structure of these particles that are not contrast matched. Therefore, these data can be used to gain information on the single particle response in crowded environment.

2.3.2 Instruments

The small-angle neutron scattering measurements, using the D11 instrument at the Institut Laue-Langevin (ILL, Grenoble, France), were performed at three configurations: sample detector distance, $d_{SD} = 34\,m$ with $\lambda = 0.6\,nm$; $d_{SD} = 8\,m$ with $\lambda = 0.6\,nm$; and $d_{SD} = 2\,m$ with $\lambda = 0.6\,nm$. Due to the velocity selector, the resolution in λ was 9%. The instrument was equipped with a ^{3}He detector with a pixel size of 7.5 mm.

Also SANS-I instrument at SINQ, Paul Scherrer Institut (Villigen, Switzerland) has been used. The q-range of interest is cover using two configurations: $d_{SD} = 18$ m with $\lambda = 0.8$ nm and $d_{SD} = 4.5$ m with $\lambda = 0.8$ nm This instrument is equipped with ^{3}He detectors with 128×128 pixels. The λ-resolution is 10%.

The measurements performed with KWS-1 and KWS-2 instruments operated by JCNS at the Heinz Maier-Leibnitz Zentrum (MLZ, Garching, Germany), were performed at three configurations to cover the q-range of interest: $d_{SD} = 20\,m$ with $\lambda = 1\,nm$; $d_{SD} = 8\,m$ with $\lambda = 0.5\,nm$; and $d_{SD} = 2\,m$ with $\lambda = 0.5\,nm$. The resolution in λ was 10%. The instrument was equipped with a ^{3}He detector with a pixel size of < 8 mm.

In Table 2 it is reported which instrument has been used to measure the different samples. It is also indicated in which other publications the data are shown. All samples have been measured at a constant temperature of 20.0 ± 0.1 °C, i.e. all the microgels were in a good solvent.

2.3.3 Form factor model

The most accepted model to fit scattering data relative to microgels has been developed almost two decades ago [11], and has been shown to correctly capture the total radius of these particles even when compared to more sophisticated models [52]. Here this model is used to obtain the variation of the microgels radius as a function of the generalized volume fraction. The microgel is approximated as a hard sphere of radius R_c, convoluted with a Gaussian decay of width 2σ to simulate the decrease of the polymer density form the center to the periphery of the microgels. The total radius of the microgels is always computed as $R = R_c + 2\sigma$. In diluted conditions when the microgels are neither compressed nor deformed the total radius is indicated as R_0 in Table 2. In contrast, when the total size of the microgels is measured with the contrast variation in concentrated solutions it is indicated as $R(\zeta)$.

The form factor of a monodisperse fuzzy sphere is described as:

$$P_1 = \left[\frac{3(\sin qR_c - qR_c \cos qR_c)}{(qR_c)^3} \exp\left\{ -\frac{(\sigma q)^2}{2} \right\} \right]^2. \quad (3)$$

To account for size polydispersity, this form factor is multiplied by a Gaussian distribution for the core radius with standard deviation $p \cdot R_c$:

$$D(R_c) = \frac{1}{\sqrt{2\pi} p \langle R_c \rangle} \exp\left[-\frac{(R_c - \langle R_c \rangle)^2}{2(p\langle R_c \rangle)^2} \right], \quad (4)$$

where now $\langle R_c \rangle$ is the mean core radius of a microgel and p is the relative with of the size distribution.

For wave-vector $q \gtrsim \pi/\sigma$, small-angle scattering can probe length-scales comparable to the inhomogeneities within the polymeric network. This contribution to the scattering is considered by adding a Lorentzian term to the scattered intensity, $I_{\text{chain}}(q) = I_{chain}(0)/[1+(\xi q)^2]$, where ξ and $I_{chain}(0)$ are a correlation length related to the mesh size of the polymer network and the zero-q intensity contribution of the internal mesh, respectively [8,55]. Therefore, the form factor model for microgels can be written as:

$$P(q) = \frac{1}{\langle V^2 \rangle} \int_0^\infty dR_c D(R_c) V^2(R_c) P_1(R_c, q) + I_{\text{chain}}(q) + B \quad (5)$$

In Equation 5, $V(R_c) = 4\pi R_c^3/3$ is the volume of the core and $\langle V^2 \rangle = \int_0^\infty dR_c V^2(R_c) D(R_c)$ represents the average squared core volume. The constant B accounts for the background due to incoherent scattering mainly due to hydrogen atoms. As mentioned in the instrument description, all SANS instruments used have a error on the value of $\lambda \approx 10\%$. The effect of the instrument resolution is a bordering of the oscillation in the form factor and can be accounted by multiplying the $P(q)$ with a Gaussian [56]:

$$P_s(q) = \frac{1}{\sqrt{2\pi}\sigma_r(q)} \int_0^\infty dq' \exp\left[-\frac{(q-q')^2}{2\sigma_r^2(q)} \right] P(q') \quad (6)$$

In the previous equation $\sigma_r^2(q)$ depends on q and account for the wavelength resolution, the geometrical resolution, and the downward-shift of the neutron beam due to gravity [57]. The values of $\sigma_r(q)$ are computed and provided together with the collected data. The fitting parameters of the model in Equation 6 are: radius of the core, R_c, width of the fuzzy shell, 2σ, width of the Gaussian distribution for the size polydispersity, pR_c, the microgel mesh size, ξ, the scale factor, $I_{chain}(0)$, and the background, B.

3 Results and discussion

3.1 Viscosimetry and generalized volume fraction

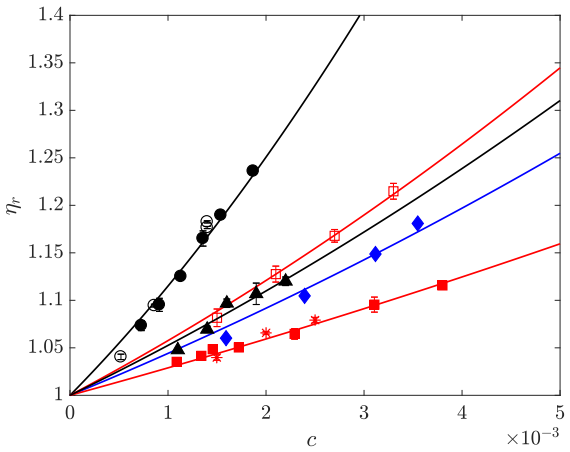

Fig. 2 Relative viscosity, η_r, as a function of the weight fraction of microgels suspended in double distilled milli-Q water, c, for: regular hydrogenated 5 mol% crosslinked microgels $H,5\%-A$ (solid diamonds) and $H,5\%-B$ (solid squares); regular deuterated 5 mol% crosslinked microgels $D,5\%$ (empty squares); ultra-low crosslinked hydrogenated microgels ULC_H (solid circles); ultra-low crosslinked deuterated microgels ULC_D (solid triangles). Empty black circles represent the values of η_r for solution of ULC_H suspended in a mixture of 55 wt% heavy water and 45 wt% double distilled milli-Q water. Red stars represent the values of η_r for solution of $H,5\%-B$ suspended in a mixture of 90 wt% heavy water and 10 wt% double distilled milli-Q water. The solid lines are fits of the data with the Einstein-Batchelor equation [58]. All measurements have been conducted at $T = 20.0 \pm 0.1$ °C.

As mentioned above, the most common method to access the generalized volume fraction of microgels is to fit the relative viscosity of highly diluted solutions of microgels with the Einstein-Batchelor equation and obtain the conversion constant k [1,23,43]. Examples of these measurements for regular 5 mol% crosslinked microgels (squares and diamonds) and ultra-low crosslinked microgels (circles and triangles) suspended in double distilled milli-Q water are shown in Figure 2. The solid lines correspond to the data fits. The values obtained for the conversion constant k for the different microgels presented here are reported in Table 1.

The black empty circles represent the values of the relative viscosity for solutions of ultra-low crosslinked microgels suspended in a mixture of 55 wt% heavy water and 45 wt% water. The red stars represent the 5 mol% crosslinked microgels, named $H,5\%-B$, suspended in a mixture of 90 wt% heavy water and 10 wt% water. These two additional solvents have been chosen since they are the solvents used for the small-angle neutron scattering experiments. It is known that microgels suspended in heavy water swell more than microgels suspended in water [59]. The fit of the viscosity data for the ULC microgel leads to a conversion constant of 44.8 ± 0.9 in pure water and 43 ± 1 in the mixture

with 55 wt% heavy water. For the 5 mol% crosslinked microgels - $H,5\%-B$ - the value of k is 11.2 ± 0.3 in pure water and 12 ± 1 in the mixture with 90 wt% heavy water. This means that the variation of the radius for the swollen microgels in heavy water has no impact on the value of the conversion constant k. A similar conclusion was already suggested by Lopez and Richtering based on the determination of the molecular weight of microgels suspended in different solvents[44]. The fact that a larger swollen size does not increase the value of the conversion constant seems counter intuitive - after all, a larger particle occupies more volume. Though, it must be considered that not only the swollen size determines the value of the conversion constant but also the collapsed size and the solvent density[2]. The different solvent used leads also to a larger collapsed size and changes the solvent density. The changes in the values of these three parameters due to the change of solvent are counterbalanced and, therefore, the conversion constant is not affected, as shown by Figure 2.

3.1.1 Effect of potential residual water on the determination of the generalized volume fraction

As mentioned in section 2.1 the presence of residual water within the freeze-dried microgels cannot be completely excluded. Nevertheless, the following discussion outlines why this does not affect the results of either this or previous studies. The precise knowledge of the mass of polymer added is fundamental if we want to use this quantity together with the microgel molecular weight to obtain the number of particles. This is of great interest in the study of microgel monolayers at liquid-liquid interfaces[33,39]. For the present work - and the previous studies in the literature - it is important to determine the relation between mass of freeze-dried microgels experimentally weighted in the realization of the solutions, c, and the generalized volume fraction. This is done by finding the relation between c and the solution viscosity and fitting the data as described in the manuscript. To see the impact of the potential residual water in the freeze-dried microgels on the values of the conversion constant and on the values of the generalized volume fraction, let us consider how the weight fraction of all the solutions is defined:

$$c = \frac{m}{m + m_{solvent}} \tag{7}$$

where m and $m_{solvent}$ are the mass of freeze-dry polymer and solvent experimentally weighted during the preparation of microgel solutions, respectively. Let's assume now that some weight concentration of residual water, c_{res}, is present in the mass m. The real mass of microgel is $m_{pNIPAM} = (1-c_{res})m < m$. Therefore, the concentration corrected for the residual water is:

$$c^\star = \frac{m_{pNIPAM}}{m + m_{solvent}} < c \tag{8}$$

As an example, c_{res} equal to 10 and 5 wt% is considered in the following. In Figure 3, equation 9 is used to rescale c into $c^\star$ for the microgel $H,5\%-B$. The red diamonds and the light blue triangles correspond to the same values of the viscosity plotted vs. concentrations of microgels rescaled assuming c_{res} equal to 10 (light blue triangle) and 5 wt% (green diamond), respectively.

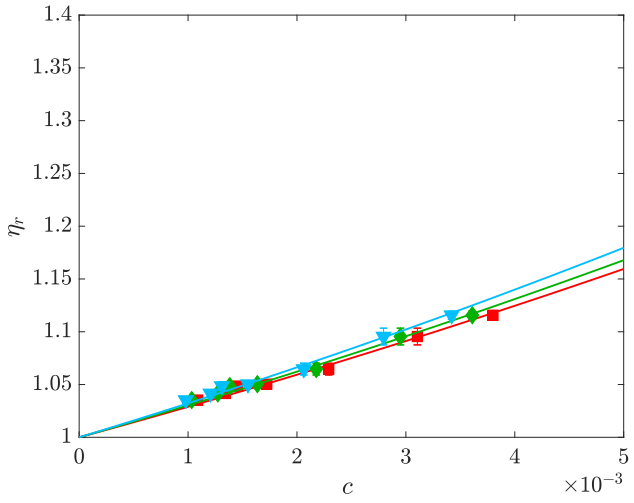

Fig. 3 Relative viscosity, eta_r vs. concentration of microgel in solution considering 0 (red square), 5 (green diamond) and 10 wt% residual water (light blue triangle) in the mass of the freeze-dried polymer. The solid lines are fit of the data with the Einstein-Batchelor equation.

For 5 wt% residual water, the fit of the data (green curve) leads to a value of $k^\star_{5\%} = 11.7\pm0.3$. In the case that 10 wt% residual water is present in the mass of the polymer, the value of the fit of the data (light blue curve) is $k^\star_{10\%} = 12.5\pm0.3$. Here it is important to notice that the values of η_r are measured and are independent to the assumption on the residual water. The values of η_r are only dependent on the volume occupied by the N swollen microgels contained in the mass m of powder weighed out. Of course, the assumption of different residual water contents shifts the concentrations, $c^\star$, to lower values - Equation 9. As a consequence, the values of k increases with increasing c_{res}.

The values of $k^\star$ obtained from the fits in Fig. 3 for different c_{res} can be used to compute the generalized volume fraction $\zeta^\star = c^\star k^\star$. Since all the concentrated solutions have been realized by suspending the very same freeze-dried polymers, the values of the added masses - and consequently their concentrations c must be rescaled considering 5 or 10 wt% residual water to obtain $c^\star < c$. Once we multiply these rescaled values of the concentration, $c^\star$ by the larger conversion constants, $k^\star$, obtained from the fits in Figure 3 the increase in $k^\star$ compensates the decrease in c and the values of $\zeta^\star$ differs less than 0.5% with respect to the values computed ignoring the residual water. The situation is completely different if m is used to compute the exact number of microgels N in solution. In this case, c_{res} must be known precisely to avoid an overestimation of N. Since here the focus is on the generalized volume fraction, the correction in Equation9 can be ignored and the mass concentration can be computed using Equation 7 since this do not affect the final estimation of ζ.

3.2 Form factors from concentrated suspensions

All the solutions measured by SANS are suspended in a solvent that matches the scattering length density of the deuterated mi-

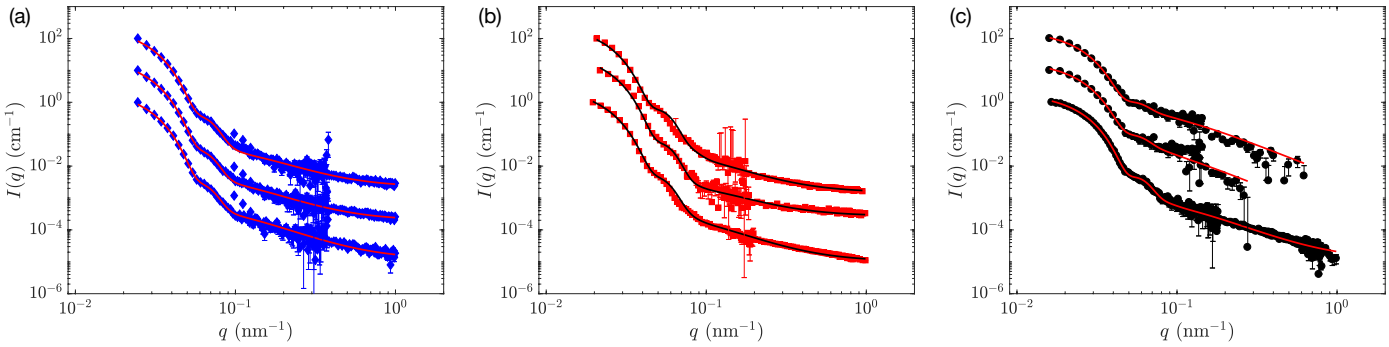

Fig. 4 Small-angle neutron scattering intensities, $I(q)$, versus scattering vector, q. (a) regular hydrogenated 5 mol% crosslinked microgels $H,5\%-A$ (solid diamonds) at different concentrations: $\zeta = 0.080 \pm 0.002$ (bottom diamonds); $\zeta = 0.60 \pm 0.01$ (middle diamonds); $\zeta = 0.70 \pm 0.01$(top diamonds); (b) regular hydrogenated 5 mol% crosslinked microgels $H,5\%-B$ (solid diamonds) at different concentrations: $\zeta = 0.080 \pm 0.002$ (bottom squares); $\zeta = 0.60 \pm 0.01$ (middle squares); $\zeta = 0.78 \pm 0.01$ (top squares); (c) Ultra-low crosslinked microgels ULC_H at different concentrations: $\zeta = 0.080 \pm 0.003$ (bottom circles); $\zeta = 0.593 \pm 0.007$ (middle circles); $\zeta = 0.697 \pm 0.009$ (top circles). All measurement were taken at $T = 20.0 \pm 0.1$ °C. Solid lines represent fits of the data with the models for a fuzzy-sphere [11]. All middle and top curves are shifted in the y-direction for clarity.

crogels that compose the concentrated matrix in which a few hydrogenated, but otherwise identical, microgels are embedded. All the 5 mol% crosslinked microgel solutions are suspended in 90 wt% heavy water - 10 wt% H_2O water solvent. In contrast, the ultra-low crosslinked microgel solutions are suspended in 55 wt% D_2O - 44 wt% H_2O solutions. In the literature, it is shown that these solvents match the scattering length densities of the deuterated microgels [3,19,23,29]. The use of two different mixtures of water and heavy water is due to the fact that deuterated ultra-low crosslinked microgels must be synthesized using a monomer that has only three atoms of deuterium instead than the usual monomer used to obtain deuterated crosslinked microgels that has seven atoms of deuterium and, consequently, a different contrast (Table 1). It has been shown that the self crosslinking of pNIPAM, responsible for the formation of the polymeric network of the ultra-low crosslinked microgels, is suppressed once the isopropyl group of NIPAM is deuterated as in the case of $[C_6D_7H_4NO]_n$ [41]. All the measurements have been performed at a temperature of 20.0 ± 0.1 °C for which the microgels are expected to be in their swollen state.

As shown in Figure 1, SANS with contrast variation allows the particle form factor as a function of the generalized volume fraction, $P(q,\zeta)$, to be accessed. This technique has indeed been used to probe the variation of the size and the structure of microgels in concentrated solution as a function of crowding [3,19,22,23,29,30].

Figure 4 shows data relative to 5 mol% crosslinked microgels, $H,5\%-A$ in (a) and $H,5\%-B$ in (b), and ULC microgels ULC_H in (c). It is clear that, even at high concentrations, only the signal of the hydrogenated microgels is visible without signs of structure peaks at low q. In a previous study [3], the fits of the data relative to the ultra-low crosslinked microgels have been used to study the structural changes in the microgel architectures with increasing ζ. The fit with the model in Equation 6 reveals that first the length of the external fuzzy shell, 2σ, decreases and is completely collapsed at $\zeta \gtrsim 0.85$, and then, at high packing fraction, also the core start to be compressed. The data on the response of individual microgels were combined with small-angle X-ray scattering measurements that probe the microgel-to-microgel arrangement. The main finding of this previous study is that the ULC softness stabilize body centered cubic (bcc) crystals which coexist with face centered cubic (fcc) crystals. The latter are the one expected for hard-spheres and hard-microgels. The bcc lattice was observed to be metastable in the literature [46,48] and its stability has now been rationalized considering the observed coexistence between faceting/interpenetration and deswelling of these supersoft microgels. The mentioned work is just an example of the many studies [1,2,6,47,60–62] conducted on the phase behavior of microgels, in analogy to hard colloids, using the generalized volume fraction.

As mentioned above, the real variable that determine the suspension phase behavior is the volume fraction ϕ. Therefore, here the focus is on the changes of the total size of microgels, $R_c + 2\sigma$, and not on the variation of their internal architecture investigated elsewhere in the past years [19,22,23,29,35]. For this study, the most important result of the fits of the SANS intensities is that the total radius of the microgels and, therefore, the volume of the microgels as a function of the generalized volume fraction, $v(\zeta)$, can be directly measured. This approach has never been used before to extensively investigate the real volume occupied by microgels in solution as a function of microgels softness. The results of the fits for the total radii of the microgels shown here and from previous publications [3,19] are reported in Table 2.

3.3 Mapping of ζ on ϕ

From the results of the fits the total radius of the particle as a function of the generalized volume fraction - $R(\zeta)$ - and, therefore, the volume of the microgels at different concentrations, $v(\zeta)$, can be obtained and used to compute the real volume occupied by the microgels in the suspensions:

$$\phi = \frac{v(\zeta)}{v_0}\zeta \tag{9}$$

The black full circles in Figure 5 represent the rescaled values of ϕ as a function of ζ computed using Equation 9 and the val-

Table 2 Results for the total radius, $R_c+2\sigma$, of the data fits from this study and from previous studies of the same microgels in the literature[3,19]. R_0 and $R(\zeta)$ corresponds to the radii computed in dilute conditions or in concentrated suspensions by means of SANS with contrast variation, respectively. In the last column is reported the instrument used to perform the SANS measurements and if the data comes from previous publications.

Name	BIS (mol%)	ζ	R_0 (nm)	$R(\zeta)$ (nm)	Instrument
ULC_H	0	0.555 ± 0.004	136 ± 2	134 ± 2	D11
ULC_H	0	0.593 ± 0.007	136 ± 2	135 ± 3	KWS1[3]
ULC_H	0	0.661 ± 0.008	136 ± 2	133 ± 4	D11[3]
ULC_H	0	0.697 ± 0.009	136 ± 2	132 ± 4	KWS1[3]
$H,5\%-A$	5	0.20	130 ± 2	129 ± 2	SANS I
$H,5\%-A$	5	0.40	130 ± 2	129 ± 1	SANS I
$H,5\%-A$	5	0.51	130 ± 2	130 ± 2	SANS I
$H,5\%-A$	5	0.60	130 ± 2	130 ± 1	SANS I
$H,5\%-A$	5	0.70	130 ± 2	126 ± 2	SANS I
$H,5\%-A$	5	0.80	130 ± 2	126 ± 1	SANS I
$H,5\%-A$	5	0.90	130 ± 2	122 ± 2	SANS I
$H,5\%-B$	5	0.56	154 ± 3	151 ± 2	KWS2
$H,5\%-B$	5	0.60	154 ± 3	153 ± 3	KWS2
$H,5\%-B$	5	0.64	154 ± 3	152 ± 2	KWS2[19]
$H,5\%-B$	5	0.78	154 ± 3	148 ± 1	KWS2
$H,5\%-B$	5	1.00	154 ± 3	137 ± 2	KWS2[19]

ues of the radii, $R(\zeta)$ in Table 2, of the hydrogenated ultra-low crosslinked microgels embedded in the matrix of deuterated, but otherwise identical ULC microgels. The course of $R(\zeta)$ vs. ζ can be used to extrapolate the expected values of the radii of the microgels at concentrations that have not been measured directly by SANS with contrast variation. With these extrapolated values of the sizes of the microgels, the generalized volume fraction of solution composed purely by hydrogenated microgels can be mapped on ϕ. These data are shown as empty circles in Fig. 5 and are taken from a previous study[3]. It can be seen that the data agrees with the data for ϕ obtained using the radii directly measured by means of SANS with contrast variation (solid black circles).

The extrapolation of the value of radius at different ζ, and its use to rescale ζ into ϕ for solutions of microgels composed of hydrogenated ULC microgels only, relies on the fact that despite the deuteration, the two species of microgels are identical. This is the case in the present study since the deuterated and hydrogenated ultra-low crosslinked microgels used here have virtually the same swollen size in the limit of highly diluted samples. The hydrodynamic radii of the two species are $R_{h,ULC_H}=138.3\pm0.6$ and $R_{h,ULC_D}=135\pm1$, respectively. The swelling ratio, that is the ratio between the hydrodynamic radii measured by dynamic light scattering in the swollen and collapsed state, is $Q_{ULC_H}=3.28\pm0.03$ and $Q_{ULC_D}=2.52\pm0.04$ for the hydrogenated and deuterated ULC microgels, respectively. This means that these microgels have both the same size and approximately the same network elasticity[44]. Though, the deuterated ULC microgels swell a bit less and, therefore, are a bit stiffer than their hydrogenated counterpart. A further confirmation of this is represented by the difference in the conversion constants obtained from viscosimetry which are related to the swelling ratio of the microgels. This different stiffness might play a role at higher concentrations than the one studied here[10]. All measurements are performed 20 °C where both the microgels are in the fully swollen soft state and the slightly different elasticity of the polymeric networks is negligible.

Also the phase behavior of solutions of ultra-low crosslinked deuterated microgels is the same as the phase behavior of solutions of hydrogenated ultra-low crosslinked microgels: coexistence between liquid and crystals appears at $\zeta=0.717\pm0.009$ and fully crystalline samples are observed at $\zeta=0.744\pm0.009$[3]. This indicates that deuterated and hydrogenated microgels have an identical interaction potential. All these observations justify the assumption that the response to crowding of the deuterated and hydrogenated microgels used in this study is the very same in the ζ-range studied here. For this reason in Figure 5 we also plot, as empty circles, the rescaled values of ϕ for samples composed of hydrogenated microgels only[3].

For low values of ζ, the points lie on the solid line $\phi=\zeta$, this means that the microgels do not change their size and the value of ζ gives the real volume occupied by the microgels in the solution. The dash-and-dotted line in Figure 5 marks the value $\zeta=0.58$, the lowest concentration at which glass transition happens for hard spheres[63]. Above this value the radius of the ULC microgels starts to decrease and the real volume occupied by the microgels in the solution is smaller than the value given by ζ.

The solution of ULC microgels with the highest concentration plotted in Figure 5 has $\zeta=0.697\pm0.009$. For higher generalized volume fractions, we observe a significant rise of the parameter describing the size polydispersity, p, in the fuzzy-sphere model used to fit the SANS data, black points in Figure 6. This can be explained by the fact that the model in Equation 5 assumes a spherical shape for the microgels. As soon as deformations are present, the fits try to reproduce the scattering profile generated by a non-spherical object with a sphere. The only parameter that can account for the non-spherical shape is the parameter describing the size polydispersity which increases with the particle deformation. This reasoning, together with evidence of the faceting of microgels at high concentration obtained from microscopy[17,18,24] or measurements of the solution osmotic pressure[21], has been used in the literature to justify the observed rise of the parameter describing the size polydispersity at high ζ for both microgels[3,36] and microemulsion[64]. Further studies are needed to definitively prove this point, and can take advantage of the recent advances in computer simulations, which are able to properly reproduce the internal architecture and response to external stimuli and crowding of microgels[65–67]. Starting from these microgels simulated

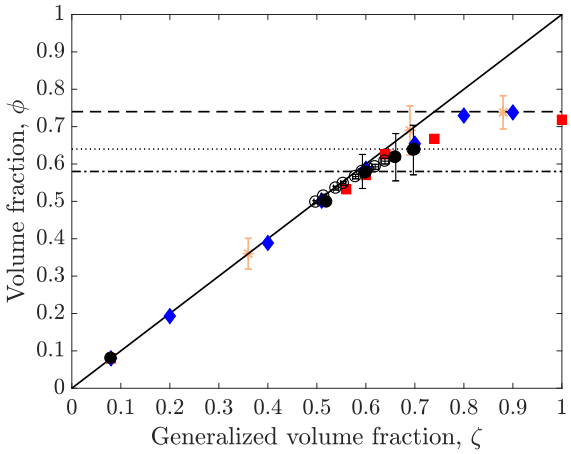

Fig. 5 Volume fraction, ϕ, as a function of the generalize volume fraction ζ for: 5 mol% crosslinked microgels $H,5\%-A$ (solid diamonds), 5 mol% crosslinked microgels $H,5\%-B$ (solid squares) and ultra-low crosslinked microgels ULC_H (circles). The solid line represent $\phi=\zeta$. The dashed line represents the maximum packing fraction of hard spheres in three dimensions ($\phi_{cp}=0.74$). The dotted line represents the value of the volume fraction for random close packed hard spheres, $\phi_{rcp}=0.64$. The dash-dotted line represents the value of the volume fraction of the glass transition for hard spheres, $\phi_{glass}=0.58$. The stars are values taken from the literature[29].

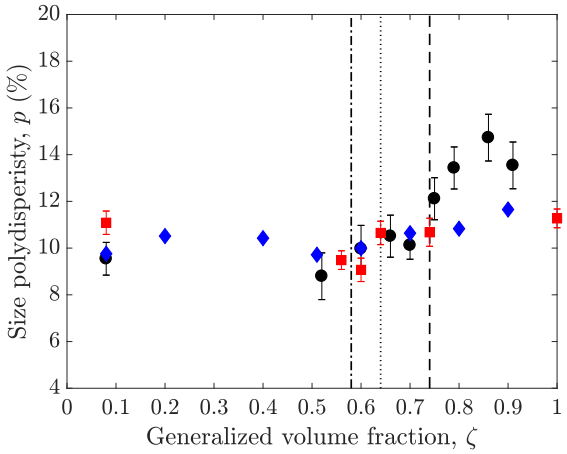

Fig. 6 Size polydispersity, p, as a function of the generalize volume fraction ζ for: 5 mol% crosslinked microgels $H,5\%-A$ (solid diamonds), 5 mol% crosslinked microgels $H,5\%-B$ (solid squares) and ultra-low crosslinked microgels ULC_H (circles). The dashed line represents the maximum packing fraction of hard spheres in three dimensions ($\phi_{cp}=0.74$). The dotted line represents the value of the volume fraction for random close packed hard spheres, $\phi_{rcp}=0.64$. The dash-dotted line represents the value of the volume fraction of the glass transition for hard spheres, $\phi_{glass}=0.58$.

in-silico, one can think to impose external deformations and generate form factors of object deformed in a controlled way. The fits of these kinds of data with the model typically used for the analysis of small-angle scattering data can quantify the relation between faceting and the increase in the parameter describing the size polydispersity. These considerations suggest that at $\zeta\gtrsim 0.74$, p increases due to the faceting of the particles and can be thought as an apparent size polydispersity.

The mapping of ϕ versus ζ for the ULC microgels reveals that ϕ, deviates from the generalized volume fraction already at $\zeta\gtrsim 0.58$. In the literature, this behavior has been shown to be due to osmotic deswelling[3,22,68]. The course of the apparent polydispersity also suggest that after a first osmotic deswelling these ULC microgels are easily deformed. The observation that already at moderate concentrations, soft microgels preferentially deform maintaining constant their volume is in agreement with a recent study on ionic microgels where the mapping of ϕ on ζ was based on measurements of the solution osmotic pressure[21]. A similar response has been recently observed by super-resolved microscopy measurements[18] and computer simulations[67]. The fact that very soft microgels start faceting at low generalized packing fraction has been rationalized considering the balance between the work needed to osmotically deswell a microgel, within the Flory-Rehner framework of gel swelling, and the work needed to deform microgels interacting with an Hertzian potential[17]. It is shown that for low osmotic pressure with respect the bulk modulus of the microgels, it is energetically favorable for the microgels to facet. In contrast, when the osmotic pressure rises up, the osmotic deswelling become favorable over faceting. The point where deswelling overtake faceting indicates that the osmotic effects of the microgel solution as a whole dominate over the mechanical deformation due to the microgel-to-microgel contacts. The dominance of osmotic deswelling over faceting depends on the characteristics of the microgels that in this approximated model are summarized by: (i) the number segments between crosslink-points (microgels synthesized with lower concentration of crosslinker agent have a larger number of segments between corsslink-points); (ii) the Kuhn length of the polymer used; (iii) the Flory-Rehner parameter. In this study, since we use pNIPAM based microgels only (i) will change between the ULC and the 5 mol% crosslinked microgels.

Now we want to see the real volume fraction occupied by harder microgels in solution. To do this, we summarize the results of experiments conducted on 5 mol% crosslinked microgels. We notice that both the deuterated ($D,5\%$) and the two hydrogenated microgels ($H,5\%-A$ and $H,5\%-B$) used for these experiments have comparable hydrodynamic radii, $R_{H,5\%-A}=153.2\pm0.5$ nm, $R_{H,5\%-B}=165\pm4$ nm, $R_{D,5\%}=153\pm1$ nm, respectively. Also the swelling ratios and, therefore, the network elasticity of these microgels are comparable: $Q_{H,5\%-A}=2.18\pm0.02$, $Q_{H,5\%-B}=1.81\pm0.06$, $Q_{D,5\%}=2.12\pm0.03$. Finally, even the phase behavior of the 5 mol% crosslinked microgels obtained from different synthesis is comparable indicating that the interaction potential can be considered the very same for all the three 5 mol% crosslinked microgels used in the ζ-range studied here.

In Figure 5, the diamonds ($H,5\%-A$) and the squares ($H,5\%-A$) represent the values of ϕ calculated using Equation 9 with $v(\zeta)$ computed using the radii of the microgels obtained from the fits of the SANS data summarized in Table 2. For these more crosslinked microgels, the relation $\phi=\zeta$ holds up to a generalized volume fraction $\zeta=0.64$, i.e. the random close packing concentration where microgels make contact with their neighbors. This

means that up to this concentration, the 5 mol% microgels do not significantly change their radius. This can be explained with the fact that the polymeric network of these microgels is harder compared to the ULC microgels as has been confirmed recently by atomic force microscopy (AFM)[32]. Consequently, their bulk modulus is larger, and higher osmotic pressures are needed to osmotically deswell or deform these particles. A similar observation was made for smaller (harder) microgels embedded in a matrix of larger (softer) microgels[22].

Once ζ rises above 0.64, the radius of the microgels decreases and the real volume fraction is smaller than ζ. In this case, given the presence of data at high ζ, a plateau for ϕ can be identified. The constant value of ϕ for 5 mol% crosslinked (harder) microgels is 0.74, that is the maximum packing fraction spheres can reach in three dimensions, dashed line in Figure 5. A similar behavior has been observed in the literature[29] and the data corresponding to these microgels are shown in Figure 5 with stars.

An important observation is that the behavior of the two 5 mol% crosslinked microgels is virtually the same even if they comes from two different synthesis and one - $H,5\%-A$ - has been synthesized with the addition of APMH. Therefore, while the addition of this monomer allows the use of fluorescent labels for super-resolved fluorescent microscopy, it does not affect the response of these microgels to crowding. Anyhow, the addition of salt to induce the blinking of the dye is needed to perform SRFM measurements and this changes the experimental conditions.

To understand if the observed deswelling is associated to faceting, the value of the parameter describing the size (or apparent for high ζ) polydispersity, p, can be monitored. This is plotted as a function of ζ in Figure 6 for the two 5 mol% microgels presented above as squares and diamonds. The values of p are virtually constant, within the experimental errors, for both the 5 mol% microgels in all the ζ-range studied here. In contrast to the ULC microgels, the 5 mol% crosslinked microgels do not facet significantly up to $\zeta \simeq 1$. This means that they deswell decreasing their volume but faceting is more limited, such that there a clear trend in the value of p vs. ζ cannot be identified in Fig. 6, and their spherical shape is mostly preserved.

To further support this observation, the values of $v(\zeta)/v_0$ as a function of ζ are shown in Figure 7. The data relative to the 5 mol% crosslinked microgels are represented by diamonds ($H,5\%-A$) and squares ($H,5\%-B$) while the circles correspond to the data of the ULC microgels (ULC_H). For the 5 mol% crosslinked microgels, the variation of the volume follows a law $\propto \zeta^{-1}$, which confirms that up to $\zeta \simeq 1$ the dominant response to crowding is isotropic compression. In contrast to both ionic microgels and softer microgels, the data reported here indicate that once the stiffness of the crosslinked network increases it is easier for the microgels to maintain their spherical shape and decrease their volume.

Figure 7 also shows that between $\zeta = 0.58$ and 0.70, the values of $v(\zeta)/v_0$ relative to the ULC microgels (circles) has a dependence on the generalized volume fraction that does not follows ζ^{-1} confirming that for soft microgels deformations play a role already at lower ζ. Points for $\zeta > 0.70$, empty circles, have been added. The values of the radii for these points are taken from a previous study[3]. As mentioned above considering in Figure 6 the increase of the values of p for the ULC microgels, these ultra-soft microgels facet at moderate ζ. This is further supported by the variation of $v(\zeta)/v_0$ for the ULC microgels shown in Figure 7, that is significantly steeper than ζ^{-1}.

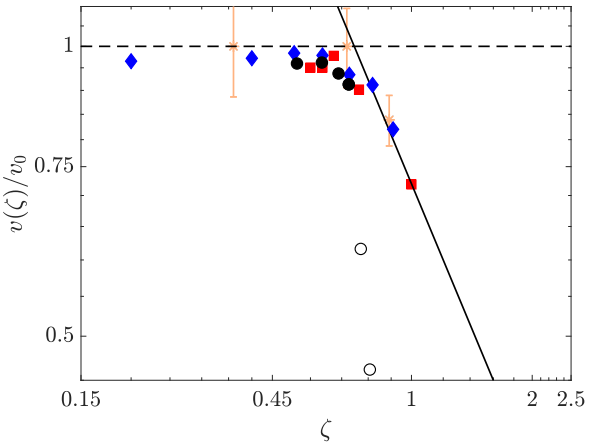

Fig. 7 Volume normalized to the swollen volume, $v(\zeta)/v_0$, as a function of the generalize volume fraction ζ for: 5 mol% crosslinked microgels $H,5\%-A$ (solid diamonds), 5 mol% crosslinked microgels $H,5\%-B$ (solid squares) and ultra-low crosslinked microgels ULC_H (circles). The solid line represent a dependence $\propto \zeta^{-1}$. The dashed line represents $v(\zeta)/v_0 = 1$. The stars are value taken from the literature[29].

4 Conclusions

This work deals with the problem of determining the real volume occupied in solution by soft deformable objects - microgels - that can facet and/or osmotically deswell depending on the concentration. To determine the real volume fraction occupied by the microgels in solution the radius of these particles is determined as a function of the solution generalized volume fraction by means of small-angle neutron scattering with contrast variation[3,19]. The study is performed on microgels with different stiffness of the polymeric network, namely ultra-low crosslinked microgels (soft) and 5 mol% crosslinked microgels (hard)[32].

It is found that soft microgels change their size already above the lowest packing fraction for which the glass transition is expected for hard spheres ($\phi = 0.58$)[63]. Therefore, already at these moderate concentrations the relation $\phi = \zeta$ breaks. Furthermore, the fits of the SANS intensities show an increase of the parameter related to the apparent polydispersity for $\zeta \ll 1$, indicating that faceting is present[3,36,64].

In contrast, for harder microgels the identity $\phi = \zeta$ holds up to a ζ for which microgels make contact with their neighbors, $\phi_{rcp} = 0.64$. This value is above the freezing and melting point for solutions of neutral crosslinked microgels[1,2,6]. Therefore, the shift to higher ζ of the onset of the liquid-to-crystal transition - freezing at $\zeta_f = 0.56$ and melting point at $\zeta_m = 0.61$, is due to the softer interaction potential with respect to the hard spheres ($\phi_f = 0.494$ and $\phi_m = 0.545$)[15], and not to an overestimation of ζ due to particle deswelling. For these hard microgels, the parameter describing the apparent polydispersity remains virtually constant

along all the ζ-range studied. This means that up to $\zeta \simeq 1$, hard microgels maintain their spherical shape and change their size, i.e. faceting is negligible.

This can be understood considering that these microgels present a more crosslinked polymeric network. The fact that the external part of 5 mol% crosslinked microgels is harder than the periphery of ULC microgels has recently been demonstrated by means of atomic force microscopy for microgels adsorbed at a solid-liquid interface[32]. Furthermore, all neutral microgels contain charges, deriving from fragments of the initiator, incorporated in the particle periphery[42]. The counter-ions associated to these charges have been reported to be responsible for the osmotic deswelling of the particles[22,68]. Therefore, at low concentrations, the harder shell resists deformation more than for softer microgels. Once the counter-ion clouds surrounding the microgels percolate the available volume between the microgels, the suspension osmotic pressure increases and becomes comparable to the microgel bulk modulus leading to the osmotic deswelling of these harder microgels. Therefore, increasing the crosslinking concentration during the synthesis makes deswelling more favorable with respect faceting, for $\zeta < 1$. In other words harder microgels prefer change their volume and maintain their shape.

Further investigations are needed to properly determine the equation of state of soft compressible microgels. The combination of small-angle neutron scattering with contrast variation and measurements of the osmotic pressure of suspensions of microgels can be a useful tool to solve this problem, and characterize the phase behavior and the flow properties of these systems as a function of ϕ. This might open to the possibility to unify some of the recent results on the flow properties of microgels[22], on their capability to create glasses and jammed state[4,7,69,70] and on their response to crowding[22,23,29].

Conflicts of interest

There are no conflicts to declare.

Acknowledgements

A. S. thanks Prof. A. Fernandez Nieves, Prof. W. Richtering and Dr. J. E. Houston for the fruitful discussions. A. S. is grateful to Dr. M. Brugnoni and Dr. S. Bochenek for the synthesis of the microgels used in this study. Financial support of the Deutsche Forschungsgemeinschaft within project A3 (Project No. 191948804) of the SFB 985 - Functional Microgels and Microgel Systems is gratefully acknowledged. The data used for this paper are available, under request, PID: XXXX. This work is based upon experiments performed at the D11 instrument at the Institut Laue-Langevin (ILL), Grenoble, France (doi.ill.fr/10.5291/ILL-DATA.9-10-1580), at the KWS-1 and KWS-2 instruments operated by JCNS at the Heinz Maier-Leibnitz Zentrum (MLZ), Garching, Germany, and at the SANS-I instrument at the Paul Scherrer Institut (PSI), Villigen, Switzerland.

Notes and references

1 H. Senff and W. Richtering, *J. Chem. Phys.*, 1999, **111**, 1705–1711.

2 A. Scotti, U. Gasser, E. S. Herman, J. Han, A. Menzel, L. A. Lyon and A. Fernandez-Nieves, *Phys. Rev. E*, 2017, **96**, 032609.

3 A. Scotti, J. E. Houston, M. Brugnoni, M. M. Schmidt, M. F. Schulte, S. Bochenek, R. Schweins, A. Feoktystov, A. Radulescu and W. Richtering, *Physical Review E*, 2020, **102**, 052602.

4 J. Mattsson, H. M. Wyss, A. Fernandez-Nieves, K. Miyazaki, Z. Hu, D. R. Reichman and D. A. Weitz, *Nature*, 2009, **462**, 83–86.

5 P. van der Scheer, T. van de Laar, J. van der Gucht, D. Vlassopoulos and J. Sprakel, *ACS Nano*, 2017, **11**, 6755–6763.

6 D. Paloli, P. S. Mohanty, J. J. Crassous, E. Zaccarelli and P. Schurtenberger, *Soft Matter*, 2013, **9**, 2927–2932.

7 C. Pellet and M. Cloitre, *Soft matter*, 2016, **12**, 3710–3720.

8 M. Stieger, J. S. Pedersen, P. Lindner and W. Richtering, *Langmuir*, 2004, **20**, 7283–7292.

9 A. Ghosh, G. Chaudhary, J. G. Kang, P. V. Braun, R. H. Ewoldt and K. S. Schweizer, *Soft matter*, 2019, **15**, 1038–1052.

10 A. Scotti, M. Brugnoni, C. G. Lopez, S. Bochenek, J. J. Crassous and W. Richtering, *Soft Matter*, 2020, **16**, 668–678.

11 M. Stieger, W. Richtering, J. S. Pedersen and P. Lindner, *J. Chem. Phys.*, 2004, **120**, 6197–6206.

12 Z. Yao, N. Grishkewich and K. Tam, *Soft Matter*, 2013, **9**, 5319–5335.

13 J. Oberdisse and T. Hellweg, *Colloid and Polymer Science*, 2020, 1–15.

14 N. F. Carnahan and K. E. Starling, *The Journal of chemical physics*, 1969, **51**, 635–636.

15 P. N. Pusey and W. Van Megen, *Nature*, 1986, **320**, 340–342.

16 W. C. Poon, E. R. Weeks and C. P. Royall, *Soft Matter*, 2012, **8**, 21–30.

17 I. B. De Aguiar, T. Van de Laar, M. Meireles, A. Bouchoux, J. Sprakel and K. Schroën, *Scientific Reports*, 2017, **7**, 1–11.

18 G. M. Conley, P. Aebischer, S. Nöjd, P. Schurtenberger and F. Scheffold, *Science advances*, 2017, **3**, e1700969.

19 A. Scotti, A. R. Denton, M. Brugnoni, J. E. Houston, R. Schweins, I. I. Potemkin and W. Richtering, *Macromolecules*, 2019, **52**, 3995–4007.

20 R. Borrega, M. Cloitre, I. Betremieux, B. Ernst and L. Leibler, *EPL (Europhysics Letters)*, 1999, **47**, 729.

21 A. Scotti, M. Pelaez-Fernandez, U. Gasser and A. Fernandez-Nieves, *Physical Review E*, 2021, **103**, 012609.

22 A. Scotti, U. Gasser, E. S. Herman, M. Pelaez-Fernandez, L. A. Lyon and A. Fernandez-Nieves, *Proceedings of the National Academy of Sciences*, 2016, **113**, 5576–5581.

23 P. S. Mohanty, S. Nöjd, K. v. Gruijthuijsen, J. J. Crassous, M. Obiols-Rabasa, R. Schweins, A. Stradner and P. Schurtenberger, *Scientific Reports*, 2017, **7**, 1487.

24 G. M. Conley, C. Zhang, P. Aebischer, J. L. Harden and F. Scheffold, *Nature communications*, 2019, **10**, 2436.

25 M. Pelaez-Fernandez, A. Souslov, L. Lyon, P. M. Goldbart and A. Fernandez-Nieves, *Physical review letters*, 2015, **114**, 098303.

26 S. Bergmann, O. Wrede, T. Huser and T. Hellweg, *Physical Chemistry Chemical Physics*, 2018, **20**, 5074–5083.

27 P. Otto, S. Bergmann, A. Sandmeyer, M. Dirksen, O. Wrede, T. Hellweg and T. Huser, *Nanoscale Advances*, 2020, **2**, 323–331.

28 O. Wrede, S. Bergmann, Y. Hannappel, T. Hellweg and T. Huser, *Soft matter*, 2020, **16**, 8078–8084.

29 U. Gasser, J. Hyatt, J.-J. Lietor-Santos, E. Herman, L. A. Lyon and A. Fernandez-Nieves, *The Journal of chemical physics*, 2014, **141**, 034901.

30 S. Nöjd, P. Holmqvist, N. Boon, M. Obiols-Rabasa, P. S. Mohanty, R. Schweins and P. Schurtenberger, *Soft Matter*, 2018, **14**, 4150–4159.

31 A. P. Gelissen, A. Oppermann, T. Caumanns, P. Hebbeker, S. K. Turnhoff, R. Tiwari, S. Eisold, U. Simon, Y. Lu, J. Mayer *et al.*, *Nano letters*, 2016, **16**, 7295–7301.

32 M. F. Schulte, S. Bochenek, M. Brugnoni, A. Scotti, A. Mourran and W. Richtering, *Angewandte Chemie International Edition*, 2020, DOI: 10.1002/anie.202011615.

33 S. Bochenek, A. Scotti, W. Ogieglo, M. A. Fernandez-Rodriguez, M. F. Schulte, R. A. Gumerov, N. V. Bushuev, I. I. Potemkin, M. Wessling, L. Isa *et al.*, *Langmuir*, 2019, **35**, 16780–16792.

34 F. Camerin, N. Gnan, J. Ruiz-Franco, A. Ninarello, L. Rovigatti and E. Zaccarelli, *Physical Review X*, 2020, **10**, 031012.

35 A. Scotti, M. Brugnoni, A. Rudov, J. Houston, I. Potemkin and W. Richtering, *The journal of chemical physics*, 2018, **148**, 174903.

36 A. Scotti, A. R. Denton, M. Brugnoni, R. Schweins and W. Richtering, *Phys. Rev. E*, 2021, **103**, 022612.

37 A. Scotti, S. Bochenek, M. Brugnoni, M.-A. Fernandez-Rodriguez, M. F. Schulte, J. E. Houston, A. P. H. Gelissen, I. I. Potemkin, L. Isa and W. Richtering, *Nature communications*, 2019, **10**, 1–8.

38 M. Andersson and S. L. Maunu, *J. Polym. Sci. :Part B: Polym. Phys.*, 2006, **44**, 3305–3314.

39 S. Bochenek, A. Scotti and W. Richtering, *Soft Matter*, 2021, **17**, 976–988.

40 X. Hu, Z. Tong and L. A. Lyon, *Colloid and polymer science*, 2011, **289**, 333–339.

41 M. Brugnoni, A. C. Nickel, L. C. Kröger, A. Scotti, A. Pich, K. Leonhard and W. Richtering, *Polymer Chemistry*, 2019, **10**, 2397–2405.

42 R. Pelton and P. Chibante, *Colloids and surfaces*, 1986, **20**, 247–256.

43 G. Romeo, L. Imperiali, J.-W. Kim, A. Fernandez-Nieves and D. A. Weitz, *The Journal of Chemical Physics*, 2012, **136**, 124905.

44 C. G. Lopez and W. Richtering, *Soft Matter*, 2017, **13**, 8271–8280.

45 P. Segre, S. Meeker, P. Pusey and W. Poon, *Physical review letters*, 1995, **75**, 958.

46 U. Gasser, J.-J. Liétor-Santos, A. Scotti, O. Bunk, A. Menzel and A. Fernandez-Nieves, *Physical Review E*, 2013, **88**, 052308.

47 S. Paulin, B. J. Ackerson and M. Wolfe, *Journal of colloid and interface science*, 1996, **178**, 251–262.

48 P. Mohanty and W. Richtering, *J. Phys. Chem. B*, 2008, **112**, 14692–14697.

49 F. S. Varley, *Neutron news*, 1992, **3**, 29–37.

50 A. Banc, C. Charbonneau, M. Dahesh, M.-S. Appavou, Z. Fu, M.-H. Morel and L. Ramos, *Soft Matter*, 2016, **12**, 5340–5352.

51 J. D. Nickels, J. Atkinson, E. Papp-Szabo, C. Stanley, S. O. Diallo, S. Perticaroli, B. Baylis, P. Mahon, G. Ehlers, J. Katsaras *et al.*, *Biomacromolecules*, 2016, **17**, 735–743.

52 M. Cors, L. Wiehemeier, O. Wrede, A. Feoktystov, F. Cousin, T. Hellweg and J. Oberdisse, *Soft matter*, 2020, **16**, 1922–1930.

53 L. Arleth and J. S. Pedersen, *Physical Review E*, 2001, **63**, 061406.

54 M. Brugnoni, A. Scotti, A. A. Rudov, A. P. Gelissen, T. Caumanns, A. Radulescu, T. Eckert, A. Pich, I. I. Potemkin and W. Richtering, *Macromolecules*, 2018, **51**, 2662–2671.

55 A. Fernández-Nieves, A. Fernández-Barbero, B. Vincent and F. De Las Nieves, *Macromolecules*, 2000, **33**, 2114–2118.

56 J. S. Pedersen, D. Posselt and K. Mortensen, *Journal of Applied Crystallography*, 1990, **23**, 321–333.

57 B. Hammouda and D. F. Mildner, *Journal of Applied Crystallography*, 2007, **40**, 250–259.

58 G. K. Batchelor, *J. Fluid Mech.*, 1977, **83**, 97–117.

59 H. Shirota, N. Kuwabara, K. Ohkawa and K. Horie, *The Journal of Physical Chemistry B*, 1999, **103**, 10400–10408.

60 S. B. Debord and L. A. Lyon, *The Journal of Physical Chemistry B*, 2003, **107**, 2927–2932.

61 L. A. Lyon, J. D. Debord, S. B. Debord, C. D. Jones, J. G. McGrath and M. J. Serpe, *The Journal of Physical Chemistry B*, 2004, **108**, 19099–19108.

62 B. Sierra-Martin and A. Fernandez-Nieves, *Soft Matter*, 2012, **8**, 4141–4150.

63 G. Brambilla, D. El Masri, M. Pierno, L. Berthier, L. Cipelletti, G. Petekidis and A. B. Schofield, *Physical review letters*, 2009, **102**, 085703.

64 F. Scheffold and T. Mason, *Journal of Physics: Condensed Matter*, 2009, **21**, 332102.

65 N. Gnan, L. Rovigatti, M. Bergman and E. Zaccarelli, *Macromolecules*, 2017, **50**, 8777–8786.

66 L. Rovigatti, N. Gnan, A. Ninarello and E. Zaccarelli, *Macromolecules*, 2019, **52**, 4895–4906.

67 S. V. Nikolov, A. Fernandez-Nieves and A. Alexeev, *Proceedings of the National Academy of Sciences*, 2020, **117**, 27096–27103.

68 U. Gasser, A. Scotti and A. Fernandez-Nieves, *Phys. Rev. E*, 2019, **99**, 042602.

69 P. Van Der Scheer, T. Van De Laar, J. Van Der Gucht, D. Vlassopoulos and J. Sprakel, *ACS nano*, 2017, **11**, 6755–6763.

70 A. Ikeda, L. Berthier and P. Sollich, *Soft Matter*, 2013, **9**, 7669–7683.